Earth Planets Space, **58**, 583–593, 2006

Vulcanian eruptions with dominant single force components observed during the Asama 2004 volcanic activity in Japan

Takao Ohminato[1], Minoru Takeo[1], Hiroyuki Kumagai[2], Tadashi Yamashina[2], Jun Oikawa[1], Etsuro Koyama[3], Hiroshi Tsuji[4], and Taku Urabe[4]

[1]*Earthquake Research Institute, 1-1-1 Yayoi, Bunkyo-ku, Tokyo 113-0032, Japan*
[2]*National Research Institute for Earth Science and Disaster Prevention, 3-1 Tennodai, Tsukuba, Ibaraki 305-0006 Japan*
[3]*Asama Volcano Observatory, Earthquake Research Institute, 2125-1 Nagakura-yama, Nagakura, Karuizawa, Nagano 389-0111, Japan*
[4]*Komoro Volcano Observatory, Earthquake Research Institute, 630 Sakaho, Kamasu, Komoro 384-0061, Japan*

(Received July 23, 2005; Revised January 17, 2006; Accepted January 31, 2006; Online published May 12, 2006)

On September 1, 2004, Mt. Asama in central Japan erupted for the first time in 21 years. Between this moderate eruption and mid-November of the same year, 4 additional moderate eruptions occurred. We installed 8 broadband seismic stations in addition to the short period seismic network around the volcano and succeeded in recording the near-field seismic signals associated with the summit eruptions. The results of the waveform inversions clearly show that the force system exerted at the source region is dominated by vertical single force components. The source depths of the single force are shallower than 200 m from the bottom of the summit crater, and the order of magnitude of the single force is 10^{10}–10^{11}N. The source time history of each vertical single force component consists of two downward forces and one upward force. The initial downward force probably corresponds to the sudden removal of a lid capping the pressurized conduit. The drag force due to viscous magma moving upward in the conduit can explain the upward force. The correlation between the single force amplitudes and the amounts of volcanic deposits emitted from the summit crater are not necessarily positive, suggesting that the amount of deposits remaining within the summit crater may have played an important role in the excitation of the single force.

Key words: Asama volcano, vulcanian eruption, single force, waveform analysis.

1. Introduction

The most general representation of seismic point sources is a combination of 6 moment tensor components and 3 single force components (Aki and Richards, 1980). Fault motions and volumetric changes in the source region are examples of seismic sources represented by 6 moment tensor components and are often observed in nature. On the other hand, single force components are not frequently observed. Most of the reports on single force components in the seismic sources are associated with volcanic activities (e.g., Kanamori and Given, 1982; Kanamori *et al*., 1984; Nishimura, 1998; Takeo *et al*., 1990), landslides (Kawakatsu, 1989) or downhill sliding of glacial ice (Ekström *et al*., 2003). The results of the reports associated with volcanic eruptions are explained essentially by the downward force that is required to compensate for the upward momentum of the volcanic ejecta. The other two examples are associated with the detachment of a huge mass from country rock or glacial ice. The country rock or ice is initially pulled downward by gravity and the force originating from the mass detachment is thus in the upward direction.

As far as we know, the first report of simultaneous observation of downward and upward forces is the research done by Chouet *et al*. (2003), who deployed a dense broadband seismic network in Stromboli, Italy. After intense investigations, they concluded that the contribution of the single force components to the amplitude of the observed seismograms was 5–13%. They proposed that the observed forces could be explained by the movement of the magma column perched above the source centroid in response to the piston-like rise of a slug of gas in the conduit.

During the Mt. Asama volcanic activity in 2004, we also observed both downward and upward single forces which were separated from each other only several seconds. In that case, however, the contribution of the single force components dominated the observed waveforms. The amplitude of the signal originating from the single force components was almost equal to that of the observed waveforms.

The times used in this report are local times (JST) and the elevations are measured with respect to sea level.

2. Setting and Seismic Activity of Asama Volcano

Mt. Asama is an andesitic volcano located in central Japan (Fig. 1). The summit elevation is 2560 m above sea level, and the size of the active summit crater is 450 m in diameter and 150 m in depth. It is one of the most active volcanoes in Japan. The first eruption recorded in historic documents occurred in 685. After a 400-year period of apparent dormancy, a large-scale plinian eruption occurred in 1108 with more than 1 km^3 of volcanic ejecta. In 1783, an-

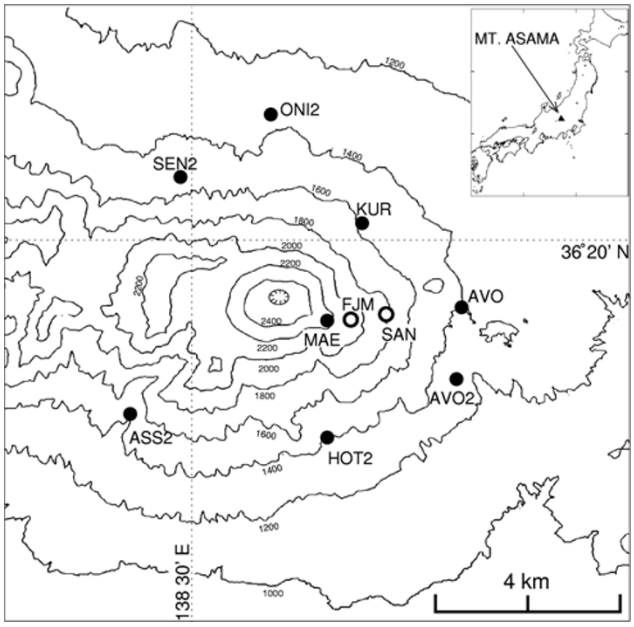

Fig. 1. Location of Mt. Asama and the seismic network. Closed circles are broadband stations. All of these stations except for AVO2 and HOT2 are equipped with short period sensors. FJM and SAN (open circles) have short period sensors only. Short period seismograms were used for the analysis of Event 1 on September 1 and Event 5 on November 14. Broadband seismograms were used for all events except for Event 1.

other plinian eruption wiped out 4 villages and killed several hundred people (Aramaki, 1963). Most of the eruptions since then have been of the vulcanian type. The last major eruptions were vulcanian and occurred during the periods 1973–1974 and 1982–1983. Mt. Asama is also famous for its role in the classification of volcanic earthquakes. The traditional classification of volcanic earthquakes based on seismogram appearance, in which earthquakes are categorized into A-type, B-type, explosion, or tremor (e.g., Minakami, 1974), was first established by the careful examination of waveforms recorded on smoked paper at Asama Volcano Observatory. To the west of Mt. Asama, there is a row of older Quaternary volcanoes collectively known as Eboshi Volcano. The volcanism near Mt. Asama appears to have progressed eastward, with Asama volcano as its eastern end and the youngest member of the row.

GPS observations showed magma injections beneath Mt. Asama from the middle of July to the end of August in 2004 (Murakami, 2004; Aoki *et al.*, 2005). The ground deformation source inferred from the GPS data was an opening of a nearly vertical dike beneath Eboshi-Asama volcanic row. Long period seismic signals with unique waveforms and a dominant period up to 10 sec had been frequently observed in the two years leading up to the eruption (Yamamoto *et al.*, 2005). An intense seismic swarm started at about 3 pm on August 31 (JMA, 2004). On September 1, the first vulcanian eruption occurred at 20:02 (JST). This eruption was accompanied by a strong air shock that was observed at stations more than 1000 km away (Fujiwara *et al.*, 2004). From September 15 to 17, Mt. Asama continuously emitted volcanic ash that reached as far as the metropolitan Tokyo about 130 km away. The largest explosion earthquake to date occurred on September 23. On September 29, October 10, and November 14, small- to moderate-scale eruptions occurred. According to the GPS observations, the opening of the dike beneath Eboshi-Asama volcanic row had continued during the volcanic activity (Aoki *et al.*, 2005). The long-period seismic activity with unique waveforms disappeared a few days before the eruption on September 1, suggesting a certain change in the volcanic edifice precursory to the following eruptions (Yamamoto *et al.*, 2005).

3. Equipment and Data

The first eruption of the Mt. Asama 2004 eruption sequence occurred on September 1 and was recorded by 5 permanent seismic stations operated by Asama Volcano Observatory (AVO), Earthquake Research Institute (Fig. 1). These permanent stations are all equipped with short period sensors except for AVO, at which a STS-2 broadband sensor is being used. On September 9, after the eruption on September 1, we added 2 more CMG-3T broadband sensors at stations MAE and KUR. Five more temporary broadband stations–stations AVO2, SEN2, and ONI2 equipped with STS-2, and stations HOT2 and ASS2 equipped with CMG-3T-started operation on September 18. All the broadband stations are digitized by the 24 bit data loggers LS7000 and LS7000XT with GPS timing manufactured by Hakusan Co. ltd. The sampling rate was 50 Hz at stations ASS2 and HOT2. 100 Hz sampling was adopted at the other broadband stations.

For the analysis of the eruption on September 1, short period records at FJM, AVO, KUR and ONI were used. Waveform records at 8 broadband stations, namely AVO, AVO2, KUR, MAE, ASS2, HOT2, ONI2 and SEN2, were used for the events on September 23 and 29. During the event on October 10, neither the three components of ASS2 nor the NS-component of SEN2 was available, due to low battery and sensor malfunction. Thus, 7 stations were operational for this event. For the event on November 14, we used two short period stations FJM and SAN in addition to 8 broadband stations. We deconvolved sensor responses of both short period and broadband records. The dominant period in the seismic signals of 5 eruptions was 2 sec. In the period range around the dominant period of 2 sec, the deconvolved seismic records both from short period sensors and from broadband sensors at the same station coincided with each other.

4. Waveform Analyses

We analyzed waveforms of all 5 explosion earthquakes (Event 1 on September 1, 20:02; Event 2 on September 23, 17:44; Event 3 on September 29, 12:17; Event 4 on October 10, 23:10 and Event 5 on November 14, 20:59) using the waveform analysis technique developed by Ohminato *et al.* (1998). Waveforms were bandpass filtered at 0.1–2 Hz. The realistic topography of the volcanic edifice and homogeneous velocity and density structures were assumed for computing Green's functions using the finite-difference method (Ohminato and Chouet, 1997). Homogeneous velocity values $V_p = 3280$ m/s, $V_s = 1660$ m/s were determined so that the observed travel times of both P and S

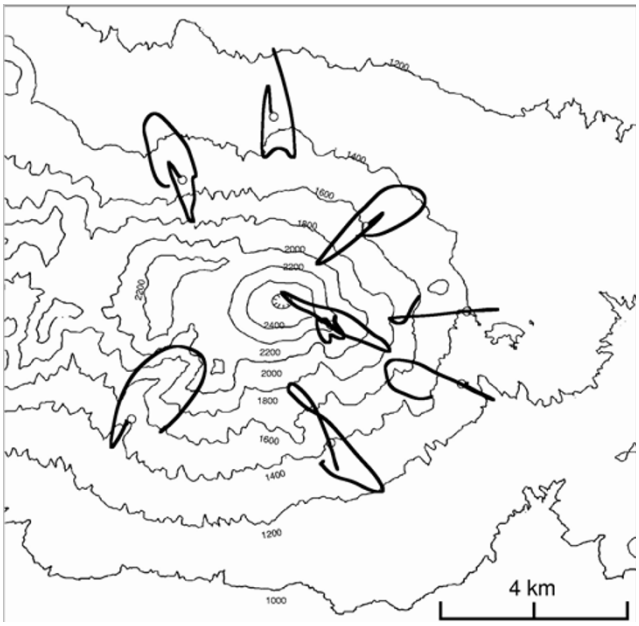

Fig. 2. Normalized particle motions of the initial 3 seconds of Event 2 on September 23 observed by the 8 broadband stations. They generally point toward the summit of Mt. Asama. Each particle motion starts from an open circle corresponding to the station location. The initial outward motions are followed by inward motions to the summit at all stations.

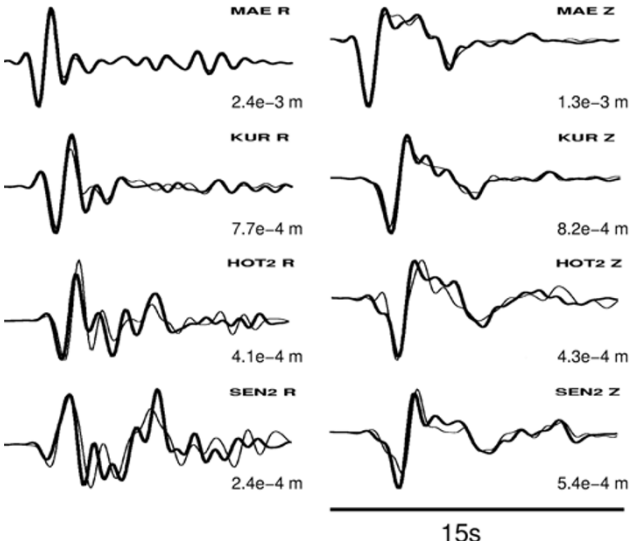

Fig. 3. Examples of the waveform match of radial and vertical displacements during Event 2 at 4 selected stations. Thick and thin lines represent observed and synthetic seismograms, respectively. The station name and component are shown at the upper right of each seismogram. A figure at the bottom right corner of each seismogram indicates the peak-to-peak amplitude of the seismogram in displacement units.

waves were minimized on average. The density value used in the analyses was $\rho = 2400$ kg/m^3.

The hypocenters of the 5 explosion earthquakes determined by the arrival times of the initial phases were distributed beneath the summit crater from 1500 to 2000 m. Horizontal particle motions generally pointed toward the same epicentral location beneath the summit crater (Fig. 2). The distribution of the small earthquakes observed just before and after the September 1 eruption determined by the double-difference technique were nearly vertical from just beneath the summit crater to the depth of -1000 m, suggesting the vertical geometry of the conduit (Yamamoto *et al.*, 2005). Keeping these hypocenter distributions in mind, we fixed the horizontal source location of the explosion earthquakes at the center of the summit crater. We then searched for and located the vertical locations of the point sources between -1000 m and 2400 m.

Since the physical processes from which single forces and force couples were originated would be different, we further assumed that the explosion source was composed of two point sources; one corresponding to three single force components and the other corresponding to 6 force couples. We examined all the possible combinations of the source depths and we located the two source depths separately.

5. Source Mechanisms and Source Time Histories

The observed waveforms were fairly well explained by the synthetic waveforms (Fig. 3). All 5 events had similar source mechanisms: a combination of single forces and an isotropic component. The vertical component of the single force components was dominant for all 5 events, and the source time histories of these vertical single force components had common features. They started with a downward force followed by an upward force. Another downward force appeared again 5–6 sec after the first downward force. These features were common to all 5 eruptions (Fig. 4). The estimated source depths and amplitudes of the single force and isotropic components are summarized in Table 1. The source depths of the single force components are shallower than 200 m from the bottom of the crater. The location of the initial downward forces at the elevations higher than the station elevations was consistent with the outward motion of the very beginning of the horizontal particle motions in Fig. 2.

5.1 Resolution of the source mechanisms

In order to confirm the existence of single force components, we examined the following five cases: Case 1, 6 moment tensor components and no single force component; Case 2, 3 single force components and no moment tensor component; Case 3, 6 moment tensor components and 2 horizontal single force components; Case 4, isotropic moment tensor components and 3 single force components; Case 5, 6 moment tensor components and 3 single force components. Variance reductions and Akaike's Information Criterion (AIC) (Akaike, 1974) for the above 5 cases for the largest eruption (Event 2) on September 23 are summarized in Table 2. Essentially the same results were obtained for the other 4 eruptions. In Fig. 5, the synthetic waveforms corresponding to the five cases are compared with a waveform recorded at MAE. The waveform matches are fairly good for Cases 2, 4 and 5, while the discrepancies between the synthetic and observed waveforms for Cases 1 and 3 are large.

Without vertical single force components (Cases 1 and 3), the variance reductions were significantly worse than in the other 3 cases that included single force components. The variance reduction in Case 2 was much larger than those in Cases 1 and 3, despite having the smallest num-

Table 1. Elevations above sea level and amplitudes of the single force and isotropic components for Events 1 through 5. Air shock amplitudes recorded by Japan Meteorological Agency at a station 8 km south of the summit crater and the mass of the volcanic deposits compiled by Yoshimoto *et al.* (2005) are also shown.

Event	Single forces		Isotropic components		Air shock	Deposits
	Elevation (m)	Amplitude (N)	Elevation (m)	Amplitude (Nm)	amplitude (Pa)	mass (kg)
1	2400	1×10^{10}	2000	1×10^{13}	205	4.9×10^{7}
2	2400	9×10^{10}	2000	5×10^{13}	72	8.5×10^{6}
3	2200	3×10^{10}	2200	2×10^{13}	30	1.3×10^{7}
4	2200	2×10^{10}	2200	1×10^{13}	19	2.8×10^{6}
5	2200	5×10^{10}	2200	7×10^{13}	73	2.5×10^{7}

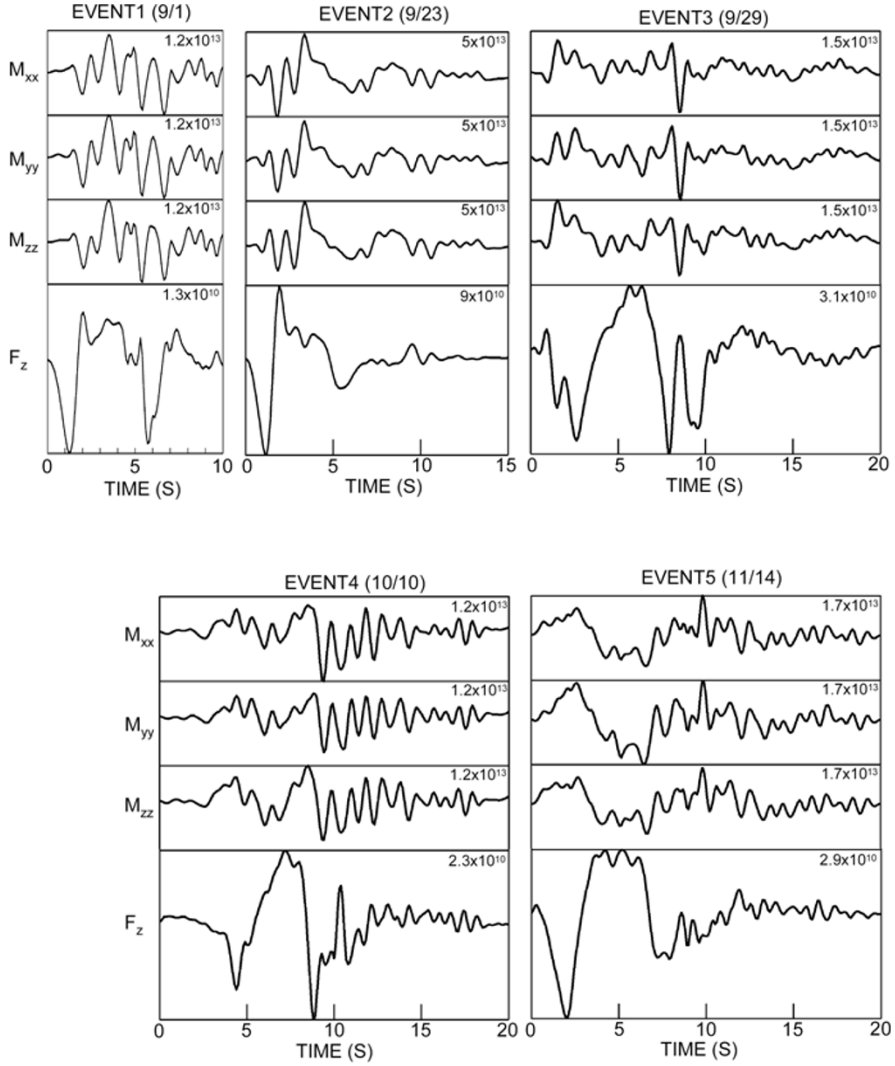

Fig. 4. Source time histories obtained by waveform inversions for the 5 events. Only the diagonal components of moment tensors and the vertical single force component are shown. Peak-to-peak amplitudes are indicated at the upper right corner of each panel. Units for the moment and force are Nm and N, respectively. Note that the amplitudes of the upward single force components are of the order of 10^{10} N.

ber of free parameters. Case 2 thus resulted in a small AIC. A large difference in AIC between Case 3 and Case 5 indicated that the vertical dipole (M_{zz}) did not compensate for the vertical single force (F_z). It is often pointed out that M_{zz} and F_z are difficult to resolve from far field data (e.g., Takeo *et al.*, 1990). In our case, however, these two components were well resolved, probably due to the proximity of our stations to the seismic source. The AIC values for Cases 4 and 5 were almost the same. This means that the off-diagonal components of the moment tensor components were negligible.

These analyses strongly support the existence of single force components. Waveform comparisons shown in Fig. 3 correspond to Case 5. The waveform matches were fairly good. Similar waveform matches were also obtained in Cases 2 and 4, as expected from their good variance reductions (Table 2). In Cases 2, 4 and 5, which included vertical single force components, the overall characteristics of the

Table 2. Variance reductions (VR) and corresponding Akaike's Information Criterion (AIC) for the 5 source mechanisms considered in the waveform analyses of Event 3. SF and ISO mean the single force and isotropic components, respectively.

	VR	AIC
Case1: 6 moment	0.358	−4574
Case2: 3 SF	0.632	−13514
Case3: 6 moment + 2 SF (Horiz.)	0.505	−7735
Case4: ISO + 3 SF	0.677	−15072
Case5: 6 moment + SF	0.758	−17737

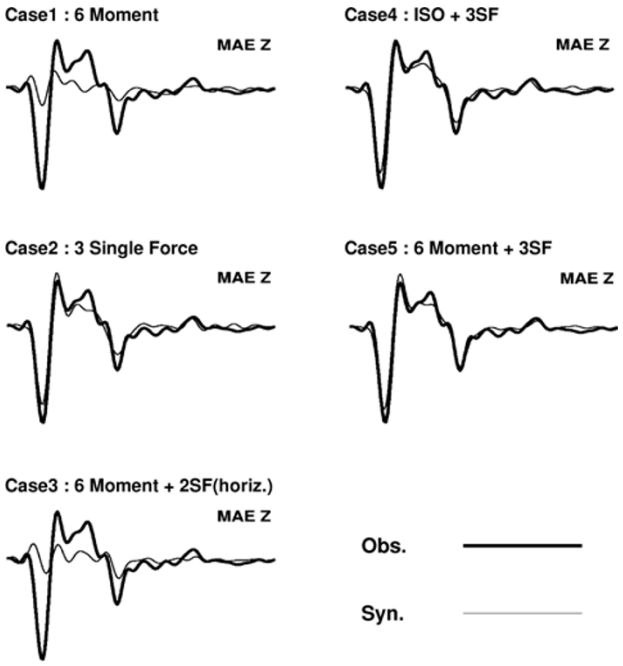

Fig. 5. Differences in waveform match for different source mechanisms corresponding to Cases 1 through 5. A single point source is assumed. Note that the waveform match in Fig. 3 was obtained by using two point sources. As an example, the vertical component recorded at MAE during Event 2 is shown. Waveform matches for the mechanisms, including the vertical single force (Cases 2, 4 and 5) are good, while the waveform matches for the other two cases are significantly poor.

time history (Fig. 4) of the single force components were shared in common.

We further conducted two numerical tests to confirm the results obtained for the real data. In the first test, synthetic seismograms for a vertical single force (F_z) at 2200 m were computed and were inverted in the same way as were the real data. For all three cases in which Green's functions associated with F_z were involved (Cases 2, 4, and 5), the synthetic waveforms were almost perfectly explained and the source time functions were well reconstructed. However, for the cases without Green's functions associated with F_z (Cases 1 and 3), the source time functions were not well reconstructed. Especially in Case 3, in which all the mechanism components except for F_z were included, the synthetic waveforms were scarcely explained. These results of the numerical test indicate that the synthetics originating from F_z are not well explained by source mechanisms other than F_z.

On the other hand, it is difficult to prove that an inversion of the synthetic seismograms computed without an F_z component does not result in a spurious F_z component in the source time function. In the second test, we computed synthetic seismograms without an F_z component and inverted them assuming all the source components including F_z. In this test, a spurious contribution from F_z was observed. But it was also observed that the variance reductions were not significantly affected by the inclusion of F_z.

When we analyzed the real data of the explosion earthquakes, the waveforms were not explained by the source mechanisms without F_z (Cases 1 and 3). However, when we analyzed the real data assuming only three single force components, the waveforms were fairly well explained (Case 2). It was also observed that a great improvement in variance reduction was obtained by the inclusion of F_z. We believe that these observations confirm the existence of the vertical single force component.

While the existence of the single force components was clearly proven, the existence of an isotropic component was somewhat ambiguous. At a distance of 1km from the source, contributions to the waveforms from a single force of 10^{10} N and a moment tensor component of 10^{13} Nm are the same. Thus, except for Event 1, the contributions of the moment tensor component to the observed seismograms are 1/3 to 1/2 of that of the single force. The obtained single force components were sensitive to depth. The total variance reduction changed significantly with changes in the source depth. If the depth of the single force components was close to the depth at which the single force components gave their minimum residual, their source time histories were stable. By contrast, the variance reduction was not significantly affected by the depth of the isotropic components, even though the source time history of the isotropic component differed from depth to depth. It is possible that the isotropic component was merely an artifact produced to explain the residual waveforms from which the contribution of single force components was removed.

5.2 Effects of spatial extension of the source

The waveform inversion technique used in the analyses is based on the point source assumption. There might be a possibility that the spatial extent of the actual source was not small compared to the dominant wavelength of the observed seismic signals, and that the obtained solutions were significantly distorted by the point source assumption. The wavelengths corresponding to a dominant period of 2 sec are approximately 6 km and 3 km for P and S waves, respectively. If the spatial extent of the source volume is only several 100 m, then the source can be treated as a point. On the other hand, if the source extent reaches several km, the solution obtained under the point source assumption may not be exact. In order to estimate the effect of the spatial extent of the source volume, we conducted the following test.

First, we computed synthetic seismograms for synchronous forces vertically distributed along the conduit at intervals of 200 m. A sine source time function $S(t) = \sin(2\pi t/t_p)$ with $t_p = 2s$ was used for the vertical single force. We investigated the range of the vertical source extension from 400 m to 3200 m. The top of the extended

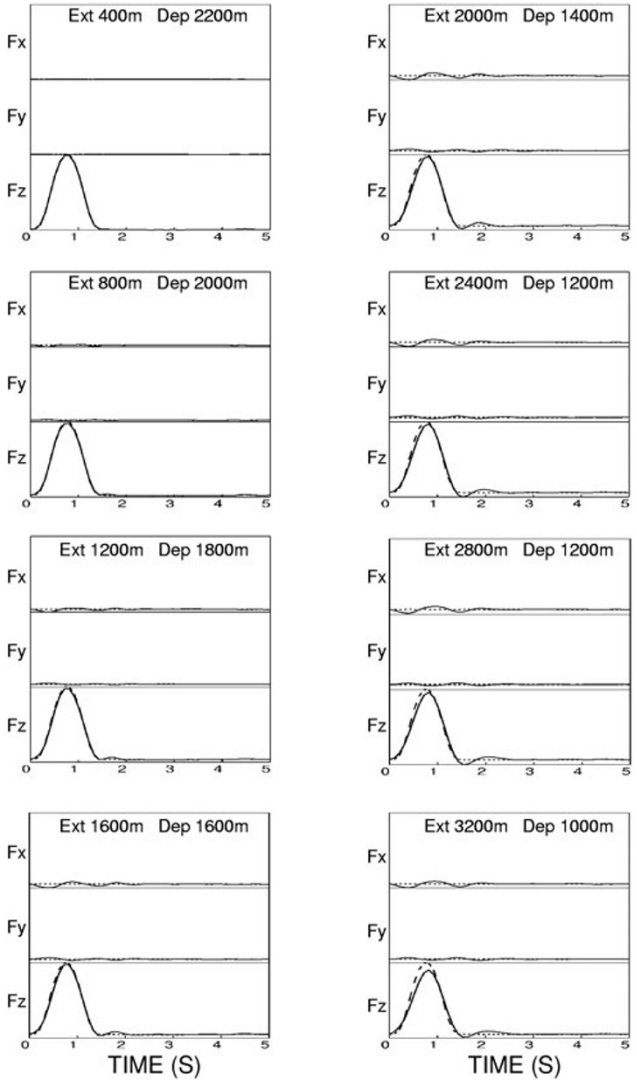

Fig. 6. Source time histories for various source lengths. Dotted lines are the given source time functions and solid lines show the results of the inversion. The vertical source length and the depth at which the best solution is obtained are shown at the top of each panel. Only single force components are shown.

source was fixed at 2400 m. Seven synthetic seismograms for point sources at 1200, 1400, 1600 1800, 2000, 2200, and 2400 m were used to mimic a vertical source extending from 1200 m to 2400 m. We then inverted the synthetic seismograms in the same manner as we did for the real data.

The source time histories for various source lengths are shown in Fig. 6. The test results are summarized as following. (1) When the source length was less than 1 km, no significant distortion of the source time function was observed. The extended source was well approximated by a point source at the center of the source extent. (2) When the source length was longer than one-half of the wavelength of the *S*-wave, a slight distortion of the source time function was observed. (3) As the source length increased, the degree of the distortion of the source time function also increased. (4) For source lengths shorter than 2800 m, the depth at which the best-fit solution was obtained coincided with the center of the source. For longer source lengths between 2800 m and 3200 m, however, the best-fit solutions were obtained at depths shallower than the center of the source, probably due to the decreasing contribution of the deep portion of the extended source to the seismograms observed at the ground surface. (5) Although the degree of the distortion increased with the source length, the source time function was not totally destroyed within the investigated range of the source length, from 400 m to 3200 m. The effect of the finite extent of the source volume was limited, and it did not generate any significant spurious forces.

6. Discussion

6.1 Origin of the vertical single force

A single force is generated by an exchange of linear momentum between the source volume and the rest of the Earth (Takei and Kumazawa, 1994). For simplicity's sake, suppose that the source volume is filled with viscous fluid and is surrounded by vertical and horizontal boundaries. When the center of mass of the internal fluid moves upward or downward by certain physical processes, such as a change in mass distribution in the source volume as a result of vesiculation or fragmentation of the fluid, then an exchange of linear momentum will take place through the boundary between the source volume and the surrounding country rock. When the viscosity of the fluid is low, the linear momentum will be exchanged mainly through the normal force on the bottom or top boundaries of the source volume. When the viscosity is high, the momentum exchange through the viscous drag force on the vertical boundary will become significant. In the following sections, we investigate the way the momentum exchange might have taken place during the explosion earthquakes at Mt. Asama.

6.1.1 Initial downward force The most plausible geometry of the source volume of the explosion earthquakes at Mt. Asama is a nearly vertical conduit filled with viscous magma. The source region was initially sealed at the top by a lid. The bottom of the source volume, on the other hand, is difficult to define because the depth reached by the magma-filled conduit is unknown. In the time history of the vertical component of single force obtained by the waveform analyses, two downward phases and one upward phase are seen. The initial downward force probably corresponds to the removal of the lid. The model used by Kanamori and Given (1982) to investigate the Mount St. Helens eruption in 1980 can be applied in explaining the generation of the initial downward single force observed at Mt. Asama.

6.1.2 Upward force: magma drain-back? The mechanism of the upward force component following the initial downward force is not easy to explain. An upward force is generated by a change of linear momentum in the downward direction, which is associated with either a downward acceleration or upward deceleration of the center of mass of the source volume. One possible physical process is a drain-back of the magma in the conduit into the deeper portion of the conduit, as was observed during the eruption of Izu-oshima volcano in 1987 (Takeo *et al.*, 1990). But the downward motion of magma in the conduit results in a gradual increase of upward force, followed by a downward force due to gradually decelerated magma movement with a relatively short time constant, as shown in figure 18 of Takeo *et al.* (1990). In addition, the magma

drain-back model does not seem to be consistent with the significant amount of volcanic ash and ejecta emitted after the initial explosion. The magma must have ascended soon after the initial explosion.

6.1.3 Upward force: viscous drag force? Another candidate for the physical process that generated the upward single force is the drag force of the ascending viscous magma applied on the very shallow portion of the conduit wall. Here, we examine whether the viscous drag force of ascending magma can quantitatively explain the observed amplitude of the upward force. The strength of the drag force F due to viscous liquid flow in a cylindrical conduit is given as $F = 8\pi\eta v l$ by the fluid viscosity η, the mean fluid velocity v and the length of the conduit wall l on which the drag force is exerted (see for example, Turcotte and Schubert, 2001).

The typical value of viscosity for andesitic magma at around 1100°C is 10^5–10^6Pas (Murase and McBirney, 1973). The effective length of the conduit wall is uncertain but is probably longer than dozens of meters and shorter than hundreds of meters. We assume 200–400 m as an estimate of the effective conduit length. It is difficult to estimate the magma ascending velocity. Rutherford and Gardner (2000) compiled typical magma ascending velocities. The averaged ascending velocities during an explosive phase are on an order of a few m/s. This rate of magma ascent is calculated from the mass eruption rates. Turcotte *et al*. (1990) theoretically estimate the exit velocity of magma-vapor mixture to be several 100 m/s for vulcanian eruptions based on the idealized one-dimensional shock-tube model. At Stromboli volcano in Italy, the gas jet velocities ranged from 40 to 100 m/s, and the velocities of the volcanic bombs derived from the gas jet velocities were around 40 m/s (Ripepe *et al*., 2001). The magma-vapor velocity or the gas jet velocity represents the velocity of fragmented magma. The magma velocity we need to know is the magma velocity before fragmentation, which may be significantly slower than the velocity of fragmented magma. Thus, these velocity values of several 10 to 100 m/s are regarded as an upper limit of the magma ascending velocity. We here assume 5–10 m/s as the magma ascending velocity. If we assume the viscosity of the andesitic magma, the fluid ascending velocity, and the effective wall length to be 10^5–10^6Pas, 5–10 m/s and 200–400 m, respectively, then the order of magnitude of the upward drag force is roughly 10^9–10^{11}N. This figure is in good agreement with the observed value.

Of course, a vertical downward force that compensates for the upward force must exist in order to preserve the total momentum. Such a downward single force may be exerted at the deeper portion of the volcanic conduit. In the case of the Asama eruptions, an exchange of linear momentum between the magma and surrounding country rock takes place probably through the viscous drag force on the vertical wall of the conduit. On the one hand, the upward force will act mainly on a relatively short portion at the top of the conduit, where the ascending velocity of magma relative to the conduit wall is large. We previously assumed that the length of that portion was several 100 m. On the other hand, since the descending velocity is low, the length of the portion of the conduit on which the descending magma exerts a downward drag force needs to be very long in order to compensate for the upward force. The downward velocity of magma in the deep portion of the conduit will be at least an order of magnitude smaller than the upward velocity of increasingly vesiculating shallow magma. The only way for the slowly descending magma to compensate the linear momentum of rapidly ascending magma would be to exert a drag force over a much longer portion of the conduit. Such a portion of the conduit starts at the depth where the relative motion between the magma and conduit wall is zero. That portion probably extends downward to a certain large depth.

Since a point source was assumed in our analyses, a force system composed of two forces, one near the surface and another at depth, may not have been well expressed by this method of analysis. Probably due to the proximity to the stations, the upward force located at the shallow part of the conduit was dominant, and the downward force that was exerted mostly in the deeper portion of the conduit was not well resolved. The closest station, MAE, is located 1.2 km from the center of the summit crater. The distance is well within the wavelength of the observed seismic signals dominated by 1–2 sec components. A force system that is composed of a shallow upward force and a deep downward force is approximated by a vertical dipole if seen from distant seismic stations. If we analyzed far field waveform data, then we might be able to obtain the force system dominated by a vertical dipole. But, probably, this idea did not work in practice. In the far field waveforms, the contribution of the dipole to the Rayleigh wave, which dominates the waveforms at large distance, would have been hidden by the contributions of the vertical downward single forces that appeared just before and after the vertical dipole force.

6.1.4 Second downward force What kind of physical mechanism could explain the second downward single force? Could it be related to the explosive fragmentation of magma in the conduit? Explosive fragmentation is a very complicated physical process. Once it begins, it is not easy to presume what kind of force system is acting on the conduit wall. One possibility is that the dominant single force component during the explosive fragmentation stage is downward. When an abrupt volume expansion of bubbles at the magma surface accelerates the upward motion of volcanic ejecta, the ejecta receive upward linear momentum. At the same time, the abrupt expansion pushes the less-fragmented magma downward in order to preserve the total linear momentum. However, it also seems possible that the dominant single force at this stage is upward. If the contribution of mass removal by an emission of ash and volcanic bombs from the conduit surpasses all other contributions, then the observed force will be upward rather than downward.

Another factor affects the direction of the single force component on the conduit wall: a change of magma viscosity in the conduit. As long as the gas fraction in the arising magma is low, an upward single force due to the arising viscous magma keeps exerting on the conduit wall. As the gas fraction of magma increases and bubbles begin interacting and coalescing, magma fragmentation begins, and the flow regime in the conduit changes from a bubbly flow

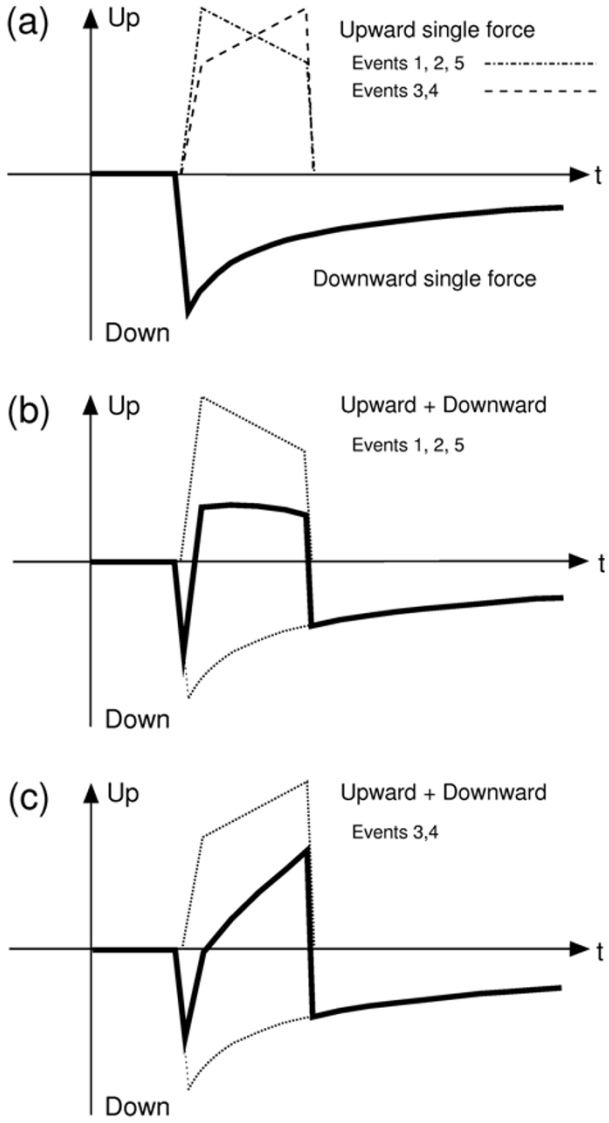

Fig. 7. (a) Time histories of a downward force and two kinds of upward forces. (b) Superposition of the downward and upward single forces for the case when magma velocity gradually decreases in the intermediate stage of the upward force. This shape resembles the observed time histories for Events 1, 2 and 5. (c) The same as (b), but the magma velocity in the intermediate stage gradually increases. This resembles the observed time histories for Events 3 and 4.

to a gas-particle/droplet flow (e.g., Dobran, 2001). Once magma fragmentation starts, the magma quickly loses its viscosity and the upward single force acting on the conduit wall becomes essentially zero. The abrupt change in magma viscosity in the conduit may explain the observed second downward single force.

According to a pressure release model by Kanamori *et al*. (1984), the time history of the vertical single force is represented by a sudden downward component followed by an gradual recovery to the initial state, as shown in Fig. 7(a). The time history of an upward force originated from the viscous drag force is subject to uncertainties. It will consist of an increasing stage corresponding to the accelerated ascent of viscous magma, and a vanishing stage corresponding to the sudden disappearance of the viscous force due to the explosive fragmentation. Between these two stages, there may be a stage where velocity does not change drastically. If we superimpose an upward single force with a time history composed of these three stages, then we obtain a time history of the single force component which qualitatively explains the characteristic time histories of the observed single force components (Figs. 7(b), (c)). According to this idea, the second downward single force is not a real force but just an apparent one. A definite answer to the origin of the second downward force remains to be studied in the future.

6.1.5 Eruption model A model of the explosion earthquakes at Mt. Asama as described above is summarized in Fig. 8. (1) Before each vulcanian eruption, the conduit sealed at the top by a lid was pressurized. The pressure in the conduit gradually increased due to a supply of volcanic gas dissolved from the magma. (2) When the pressure exceeded the lid strength, the first downward single force was initiated by a sudden removal of the top lid. (3) The magma in the conduit was depressurized, and the volume expansion of magma due to its vesiculation was initiated. As the volume of magma in the conduit increased, the magma head rose, exerting an upward drag force on the conduit wall. A downward single force was exerted at the deeper portion of the conduit in order not to violate the conservation of linear momentum. (4) The magma reached the very shallow portion of the conduit and was exposed directly to the atmospheric pressure. (5) An explosive fragmentation of magma started at the very shallow portion of the conduit. The viscosity of the magma dropped suddenly, and the upward viscous drag force on the conduit wall almost vanished. (This explanation of the second downward force is not unique, as mentioned above.)

6.1.6 Vulcanian eruptions without a dominant single force A vertical single force whose contribution to the waveforms is larger than the contribution of the moment component does not always accompany vulcanian eruptions. The mild vulcanian eruptions at Popocatépetl Volcano, Mexico were accompanied by a single force component with a magnitude of the order of 10^8 N, but the contribution of the single force to the waveforms was not dominant (Chouet *et al*., 2005). Uhira and Takeo (1994) referred to the difficulty in distinguishing the contributions of M_{zz} and F_z components to the waveforms accompanying the vulcanian eruptions at Sakurajima volcano, Japan. Tameguri *et al*. (2002) showed that the waveforms associated with the vulcanian eruptions at Sakurajima could be explained without including a single force component.

The contributions of single force components to the waveforms vary from eruption to eruption. This variance may reflect certain conditions of the volcanoes, such as the viscosity of the magma, the gas content of the magma, or the geometry of the volcanic conduit. Thus, a quantitative evaluation of single force components will give us a new insight into volcanic eruptions.

6.2 Intensity of the 2004 Asama eruption

During the 2004 Asama eruptions, acoustic and geological measurements were conducted in addition to the seismic observations. In the following, we discuss the scale of the 2004 Asama eruptions based on these different types of observations.

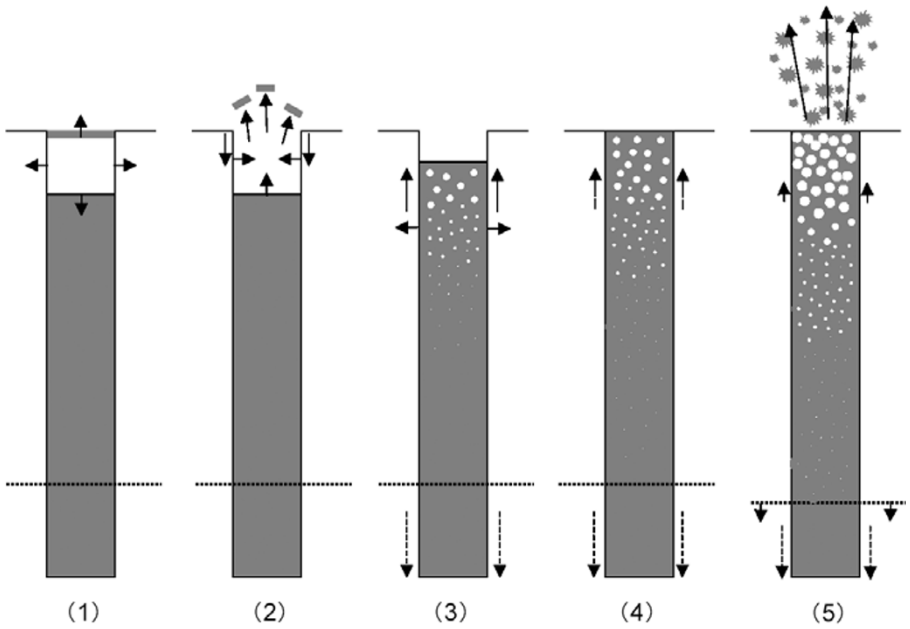

Fig. 8. Schematic model of vulcanian explosions at Mt. Asama. (1) The pressurized stage just before the eruption. The conduit is sealed at the top by a lid. (2) A sudden removal of the top lid generates the first downward single force. (3) An upward movement of magma in the conduit exerts an upward drag force on the conduit wall. (4) The magma head reaches the ground surface. (5) When the explosive fragmentation near the top of the conduit starts, the upward viscous drag force on the conduit almost disappears. The horizontal dotted line shows the descending vesiculation level.

McNutt (1994) showed that the volcanic explosive index (VEI) of Newhall and Self (1982) could be estimated based on tremor reduced displacement (D_R). He showed that the VEI value associated with the erupted volume of volcanic deposits and the $\log(D_R)$ associated with the seismic intensity were linearly related. Nishimura *et al.* (1995) showed that the source mechanism of the volcanic tremor was explained by a vertical single force. These studies suggest that the amplitude of the vertical single force component and the amount of the volcanic deposits should have had a positive correlation during the 2004 Asama eruptions. However, as shown in Table 1 and Fig. 9, their correlation was not necessarily positive. Event 1 on September 1 was the largest eruption with respect to the amplitude of the air shock and amount of volcanic deposits, while Event 2 on September 23 was far more intense than the other 4 eruptions from the viewpoint of the single force amplitude. On the other hand, the air shock intensity and amount of volcanic deposits have a positive correlation for all 5 events. We will discuss below how the complicated relation between the single force amplitude and air shock amplitude arose.

According to the eruption source model used by Kanamori *et al.* (1984), the intensity F of the vertical single force is

$$F = SP, \tag{1}$$

where S is the cross section of the conduit and P is the pressure in the conduit. The source of air shock would be a lid pushed and accelerated upward by the pressure in the conduit. Since the observed amplitudes of the air shock were inversely proportional to their distance from the vent, we assume that the source is a monopole. Then, the excess pressure p depends on the rate of mass outflow $\dot{q}$ from the source as $p = \dot{q}/4\pi r$ (e.g., Blackstock, 2000), where r is the distance from the source. The mass outflow is expressed as $\dot{q} = \rho S a$, where ρ is the air density, S is the cross section of the lid and a is the vertical acceleration of the lid. In addition, the acceleration a, the force F and the mass of the lid m are related as $F = ma$. For such a monopole source of sound in a half-space, the far-field pressure p observed at the distance r from the source is,

$$p = \frac{\rho S a}{2\pi r} = \frac{\rho S}{2\pi r}\frac{F}{m}, \tag{2}$$

Note that factor 2 is included to account for the radiation in a half-space.

The single force amplitude, the air shock amplitude, and the volcanic deposits are not necessarily positively related to each other, as shown in Fig. 9. The single force intensity

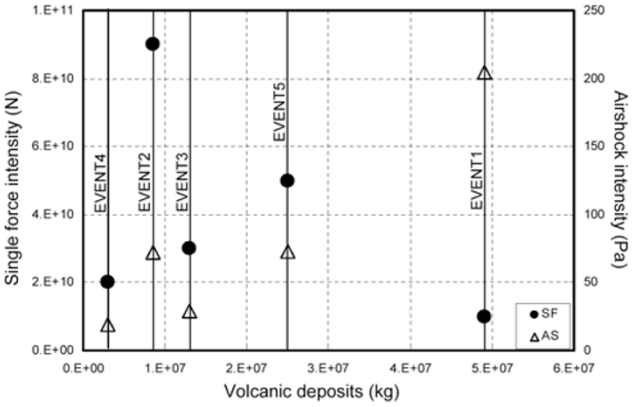

Fig. 9. Relation between mass of the volcanic deposits and the amplitude of the single forces (SF) and air shocks (AS). The single forces for Events 3, 4, and 5 and the air shock amplitudes for all 5 events align, but the single force amplitudes for Events 1 and 2 are exceptionally small and large, respectively.

for Event 2 is nine times larger than that for Event 1, while the air shock amplitude for Event 2 is only a third of that for Event 1. As shown in Eq. (1), the amplitude of the single force is proportional to the cross section of the conduit and the pressure in it. Since there is no special reason for the significant change in the cross-section S between Event 1 and Event 2, the difference in the intensity of the single force component should be attributed to the difference of the pressure P in the conduit. It was interpreted that the pressure in the conduit before Event 2 was nine times larger than that before Event 1. Nishimura and Uchida (2005) analyzed the surface waves excited by the eruptions, and obtained essentially the same conclusions.

According to Eq. (2), the air shock amplitude p is positively related to the force F, and, at the same time, inversely related to the mass of the lid m. In order to explain the air shock amplitude for Event 2, the mass of the lid for Event 2 must be nearly 30 times larger than that for Event 1. The large difference in the mass of the lid is in good agreement with the observation that the bottom of the summit crater was filled with a pancake-shaped lava mound 65 m thick before Event 2 (Oki *et al.*, 2005). The lava mound was formed after Event 1, and was partially blown off at the center of the mound during Event 2. Although the pressure in the conduit before Event 2 was 9 times higher, probably due to a sealing effect by the thick lava mound, the acceleration of the lid was only a third due to the large mass of the lid. The low acceleration of the lid resulted in the small amplitude radiation of sound. The other eruptions can be interpreted in the same manner. Events 3, 4 and 5 are characterized by moderate conduit pressure and the large mass of the lid. It is only in Event 1 among the five explosions where there was no thick lava mound before eruption.

Since some part of the lid would be blown off during each eruption, it seems natural for there to be a positive relation between the volcanic deposits and the mass of the lid. However, the observed volcanic deposits are positively related to the air shock amplitudes rather than to the lid mass. How can this be explained? How great is the uncertainty of the volcanic deposits estimation? According to the scientists who conducted the volcanic deposits measurements during the 2004 Asama eruption, it is certain that the amount of ash emitted during the September 23 eruption (Event 2) was exceptionally small. Although there may be uncertainty by a factor of several times, it is unlikely that the actual amount of emitted ash could be nearly ten times more than the amount that was actually measured (Yoshimoto, personal communication). Thus, the relation between the volcanic deposits and the mass of the lid is not explained by the uncertainty in the volcanic deposits measurements.

It is possible that only a fraction of the total substances moved during the eruptions were actually emitted as ash. Aerial photos taken just after Event 2 support this idea. These photos show that gigantic rock blocks whose estimated mass exceeds several hundred to one thousand tons (10^5–10^6 kg) were scattered in the summit crater. The number of these huge blocks was over several hundred. This means that the total mass of such huge rocks distributed inside the crater amounted to at least 10^7–10^8 kg. This mass is several to ten times more than the mass of ash emitted outside of the summit crater. In addition, it is highly possible that the shallowest portion of the conduit was filled with much larger masses of fragmented rocks and solidified magma, which moved up and down in the conduit during eruptions and contributed to the excitation of the single force. Not all of the volcanic ejecta can reach the outside of the summit crater. The volcanic deposits inside the crater have been omitted from the estimation of the mass emission. But such unmeasured materials would have occupied the great portion of the mass of the lid capping the conduit.

The mass of ash that emitted outside of the summit crater rim contributed to the mass of the volcanic deposits actually measured. Probably, the mass of ash was strongly related to the final velocity reached by the lid vertically accelerated before breaking into small volcanic ejecta. Since the air shock amplitudes are proportional to the vertical acceleration of the lid as shown in Eq. (2), the positive relation between the air shock amplitudes and volcanic deposits seen in Fig. 9 is easily understood.

7. Conclusions

We analyzed 5 explosion earthquakes during the Mt. Asama 2004 eruptions. The results of the waveform analyses indicate that a vertical single force whose depth range was 0–200 m from the bottom of the summit crater dominated the force system at the source region. The source time histories of the vertical single force are characterized by an initial downward force followed by an upward force. Another downward force was observed 5–6 sec after the first one. The initial downward vertical force can be attributed to a reaction force of the volcanic jet or volcanic ejecta. The upward single force following the initial downward force can be explained by a drag force applied to the very shallow portion of the conduit wall due to viscous fluid flow. When magma starts fragmentation and loses its viscosity, the upward force suddenly disappears. The second downward force may not be an actual force, but an apparent force due to the disappearance of the upward force. A downward force must accompany the upward force in order to preserve the total momentum. One possible reason that the downward counterpart was not observed is the point source assumption. Our next step will be to apply a method of analysis in which we can spatially resolve the distributed force system along the volcanic conduit in order to understand the detailed physical processes within the conduit during the explosive eruptions.

Acknowledgments. The authors thank the staff of ERI and NIED who made it possible for us to carry out the prompt observation. We are also grateful to M. Yoshimoto for useful discussion. Reviews by M. Ripepe and an anonymous reviewer improved the final manuscript considerably.

References

Akaike, H., A new look at the statistical model identification, *IEEE Trans. Autom. Contol*, **AC-9**, 716–723, 1974.

Aki, K. and P. G. Richards, *Quantitative Seismology, Theory and Method vol. I*, 557 pp., Freeman, New York, 1980.

Aoki, Y., H. Watanabe, E. Koyama, J. Oikawa, and Y. Morita, Ground deformation associated with the 2004–2005 unrest of Asama Volcano, Japan, *Bull. Volcanol. Soc. Japan*, **50**, 575–584, 2005 (in Japanese with English abstract).

Aramaki, S., Geology of Asama Volcano, *J. Fac. Sci. Univ. Tokyo*, **14**, 229–443, 1963.

Blackstock, D. T., *Fundamentals of Physical Acoustics*, 541 pp., Wiley-Interscience, New-York, 2000.

Chouet, B. A., P. Dawson, T. Ohminato, M. Martini, G. Saccorotti, F. Giudicepietro, G. De Luca, G. Milana, and R. Scarpa, Source mechanisms of explosions at Stromboli Volcano, Italy, determined from moment-tensor inversions of very-long-period data, *J. Geophys. Res.*, **108**, doi:10.1029/2002JB001919, 2003.

Chouet, B., P. Dawson, and A. Arciniega, Source mechanism of vulcanian degassing at Popocatépetl Volcano, Mexico, determined from waveform inversion of very long period signals, *J. Geophys. Res.*, **110**, doi:10.1029/2004JB003524, 2005.

Dobran, F., *Volcanic Processes Mechanisms in Material Transport*, 590 pp., Kluwer Academic, 2001.

Ekström, G., M. Nettles, and G. A. Abers, Glacial earthquakes, *Science*, **302**, 622–624, doi:10.1126/science.1088057, 2003.

Japan Meteorological Agency, Eruptions of Asamayama volcano in September 2004, *Abst. Volcanol. Soc. Japan 2004 Fall Meeting*, 181, 2004 (in Japanese).

Fujiwara, Y., T. Sakai, K. Kato, M. Nakamura, H. Naito, H. Yamasato, M. Churei, H. Hiramatsu, Y. Ueda, and S. Iijima, Mt. Asama eruption on 1st September 2004: Air-shock waveforms observed all over Japan, *Abst. Volcanol. Soc. Jap. 2004 Fall Meeting*, 202, 2004 (in Japanese).

Kanamori, H. and J. W. Given, Analysis of seismic body waves excited by the May 18, 1980, eruption of Mount St. Helens—a terrestrial monopole?, *J. Geophys. Res.*, **87**, 5422–5432, 1982.

Kanamori, H., J. Given, and T. Lay, Analysis of seismic body waves excited by the Mount St. Helens eruption of May 18, 1980, *J. Geophys. Res.*, **89**, 1856–1866, 1984.

Kawakatsu, H., Centroid single force inversion of seismic waves generated by landslides, *J. Geophys. Res.*, **94**, 12363–12374, 1989.

McNutt, S. R., Volcanic tremor amplitude correlated with volcano explosivity and its potential use in determining ash hazards to aviation, *USGS Bull.*, **2047**, 377–385, 1994.

Minakami, T., Seismology of volcanoes in Japan, in *Physical Volcanology Developments in Solid Earth Geophysics vol 6*, edited by Civetta *et al.*, 333 pp., Elsevier, Amsterdam, 1–27, 1974.

Murakami, M., Magma migration preceding 2004 eruption of Asama Volcano detected by GPS, *Abst. Volcanol. Soc. Jap. 2004 Fall Meeting*, 204, 2004 (in Japanese).

Murase, T. and A. R. McBirney, Properties of some common igneous rocks and their melts at high temperatures, *Geol. Soc. Am. Bull.*, **84**, 3563–3592, 1973.

Newhall, C. G. and S. Self, The volcanic explosivity index (VEI): An estimate of explosive magnitude for historical volcanism, *J. Geophys. Res.*, **87**, 1231–1238, 1982.

Nishimura, T., Source mechanisms of volcanic explosion earthquakes: single force and implosive sources, *J. Volcanol. Geotherm. Res.*, **86**, 97–106, 1998.

Nishimura, T. and H. Uchida, Application of single force model to the volcanic explosion earthquakes observed at Asama Volcano in 2004, *Bull. Volcanol. Soc. Japan*, **50**, 387–391, 2005 (in Japanese with English abstract).

Nishimura, T., H. Hamaguchi, and S. Ueki, Source mechanisms of volcanic tremor and low-frequency earthquakes associated with the 1988–1989 eruptive activity of Mt. Tokachi, Hokkaido, Japan, *Geophys. J. Int.*, **121**, 444–458, 1995.

Ohminato, T. and B. Chouet, A free-surface boundary condition for including 3D topography in the finite difference method, *Bull. Seismol. Soc. Am.*, **87**, 494–515, 1997.

Ohminato, T., B. Chouet, P. Dawson, and S. Kedar, Waveform inversion of very-long-period impulsive signals associated with magmatic injection beneath Kilauea volcano, Hawaii, *J. Geophys. Res.*, **103**, 23839–23862, 1998.

Oki, S., M. Murakami, N. Watanabe, B. Urabe, and M. Miyawaki, Topographic change of the summit crater of the Asama volcano during 2004 eruption derived from repeated airborne Synthetic Aperture Radar (SAR) measurements, *Bull. Volcanol. Soc. Japan*, **50**, 401–410, 2005 (in Japanese with English abstract).

Ripepe, M., S. Ciliberto, and M. D. Schiava, Time constraints for modeling source dynamics of volcanic explosions at Stromboli, *J. Geophys. Res.*, **106**, 8713–8727, 2001.

Rutherford, M. J. and J. E. Gardner, Rates of magma ascent, in *Encyclopedia of Volcanoes*, edited by Sigrudsson *et al.*, 1417 pp., Academic Press, San Diego, 207–217, 2000.

Takei, Y. and M. Kumazawa, Why have the single force and torque been excluded from seismic source models?, *Geophys. J. Int.*, **118**, 20–30, 1994.

Takeo, M., H. Yamasato, I. Furuya, and M. Seino, Analysis of long-period seismic waves excited by the November 1987 eruption of Izu-Oshima volcano, *J. Geophys. Res.*, **95**, 19377–19393, 1990.

Tameguri, T., M. Iguchi, and K. Ishihara, Mechanism of explosive eruptions from moment tensor analyses of explosion earthquakes at Sakurajima Volcano, Japan, *Bull. Volcanol. Soc. Japan*, **47**, 197–215, 2002.

Turcotte, D. L. and G. Schubert, *Geodynamics Second Edition*, 456 pp., Cambridge University Press, Cambridge, 2001.

Turcotte, D. L., H. Ockendon, J. R. Ockendon, and S. J. Cowley, A mathematical model of vulcanian eruptions, *Geophys. J. Int.*, **103**, 211–217, 1990.

Uhira, K. and M. Takeo, The source of explosive eruption of Sakurajima volcano, Japan, *J. Geophys. Res.*, **99**, 17775–17789, 1994.

Yamamoto, M., M. Takeo, T. Ohminato, J. Oikawa, Y. Aoki, H. Ueda, S. Nakamura, H. Tsuji, E. Koyama, N. Osada, and T. Urabe, A unique earthquake activity preceding the eruption at Asama volcano in 2004, *Bull. Volcanol. Soc. Japan*, **50**, 393–400, 2005 (in Japanese with English abstract).

Yoshimoto, M., T. Shimano, S. Nakada, E. Koyama, H. Tsuji, A. Iida, M. Kurokawa, Y. Okayama, M. Nonaka, T. Kaneko, H. Hoshizumi, Y. Ishizuka, R. Furukawa, K. Nogami, S. Onizawa, K. Niihori, T. Sugimoto, and M. Nagai, Mass estimation and characteristics of ejecta from the 2004 eruptions of Asama volcano, *Bull. Volcanol. Soc. Japan*, **50**, 519–533, 2005 (in Japanese with English abstract).

T. Ohminato (e-mail: takao@eri.u-tokyo.ac.jp), M. Takeo, H. Kumagai, T. Yamashina, J. Oikawa, E. Koyama, H. Tsuji, and T. Urabe